Signal-level Integrity and Metrics Based on the Application of Quickest Detection Theory to Interference Detection

D. Egea-Roca, G. Seco-Granados, J. López-Salcedo, *UAB*, Spain;
E. Domínguez, *GMV*, Spain;
E. Aguado, D. Lowe, *NSL*, United Kingdom;
D. Naberezhnykh, *TRL*, United Kingdom;
F. Dovis, *Politecnico di Torino*, Italy;
I. Fernández-Hernández, J.P. Boyero, *European Commission*, Belgium

BIOGRAPHY

Daniel Egea received the M.Sc. in Electrical Engineering in 2012 and the M.Sc. degree in Micro and Nano Electronics Engineering in 2013, both from Universitat Autònoma de Barcelona (UAB). Currently, he is a Ph.D. student at the Signal Processing for Navigation and Communications (SPCOMNAV) group, of UAB and his research is focused on signal-level GNSS integrity.

Gonzalo Seco-Granados holds a PhD degree from Univ. Politecnica de Catalunya (UPC) and an MBA from IESE, Universidad de Navarra. Since 2006, he is associate prof. at the Dept of Telecom. Eng. of UAB and head of the SPCOMNAV group.

José A. López-Salcedo received the M.Sc. and Ph.D. degrees in Telecommunication Engineering in 2001 and 2007 from UPC. He joined UAB and the SPCOMNAV group as an assistant prof. in 2006, and since 2013 he is an associate prof.

Enrique Domínguez received a M.Sc. in Telecommunications Engineering in 2000 and a Master in Space Technologies in 2009, both from the Polytechnic University of Madrid. He joined GMV in 2000 working first in the development of EGNOS and Galileo and since 2009 in GNSS software receivers, multi-sensor fusion and integrity algorithms.

L. Enrique Aguado is a Principal Project Manager at NSL. He received a Ph.D. in Electrical Engineering from the University of Manchester, UK. He has been involved in Galileo-related R&D since 2002 with his current work focussed on robust positioning technologies.

David Lowe is a Principal Navigation Engineer at NSL. He received a PhD in Engineering Surveying and Space Geodesy from the University of Nottingham, UK.

Denis Naberezhnykh received the BSc. degree in Physics from the Royal Holloway, University of London and is the Head of Low Carbon Vehicle and ITS technology at TRL.

Fabio Dovis received a Master degree in Electronics Engineering in 1996, and a PhD in Electronics and Communications Engineering in February 2000, at Politecnico di Torino. He is currently assistant professor at the Department of Electronics and Telecommunications of Politecnico di Torino.

Ignacio Fernández-Hernández is currently responsible for the Galileo Commercial Service at the EC. He has a M.Sc. in Electronic Engineering by ICAI, Madrid, and a MBA by London Business School.

Juan Pablo Boyero is since 2012 working at the EC in the definition of the evolution of the Galileo and EGNOS missions. He holds a MSC by the Escuela Técnica Superior de Ingenieros de Telecomunicación of the Universidad Politécnica de Madrid.

ABSTRACT

In this paper, we will concentrate on interferences as one of the major impairments that can threat the integrity of mass-market GNSS receivers. While the topic of interference detection has already been covered in the existing GNSS literature, the purpose of this work is to focus on the fast and reliable detection of interferences, using the tools of the so-called "quickest detection" theory. To do so, time plays a relevant role, since we are often interested in minimizing the time for detecting a given threat. This is in contrast to classical detection techniques, where the goal is to maximize the detection probability subject to some probability of false alarm, but where "time" is not explicitly considered.

Theoretical results on quickest detectors are complemented in this work with experimental tests using real signals, obtained in the framework of the EC funded iGNSSrx project. The effects of different types of interferences onto the proposed quickest detection techniques are shown and the performance of the designed detection algorithms working in real conditions is presented. The results show how the behavior of the proposed algorithms is satisfactory for being used in integrity monitoring applications.

INTRODUCTION

With the widespread deployment of GNSS, one of the major challenges to be solved is the provision of integrity to users beyond the civil aviation community, where this feature is already a well-established performance criterion. Position integrity is typically provided in civil aviation by Receiver Autonomous Integrity Monitoring (RAIM) algorithms and Satellite Based Augmentation Systems (SBAS). However, such methods require conditions that cannot be fulfilled in road and urban environments due to effects like multipath propagation and interference signals [1]. This implies that signal integrity, which in civil aviation is almost translated into position integrity, can hardly be used to ensure position integrity in terrestrial environments. It is for this reason that signal integrity is actually a concern within the GNSS community, motivated by the widespread deployment of terrestrial GNSS receivers and the emergence of new GNSS-based applications and services [2], specially safety of life and critical systems.

Herein, we will concentrate on interferences as one of the major impairments that can threaten the integrity of mass-market GNSS receivers. This is in line with the increasing concern on the unauthorized use of low-cost portable jammers, which have become a real threat for GNSS-based services [3], especially in road or urban environments. While the topic of interference detection has already been covered in the existing GNSS literature [4], the purpose of this work is to focus on the fast and reliable detection of interferences, using the tools of the so-called "quickest detection" theory. The output information from quickest detectors can be used either to discard the current measurements (i.e. thus avoiding outliers in subsequent stages of the receiver) or to apply mitigation techniques as soon as possible (i.e. thus bounding the performance degradation within some given limits). To do so, time plays a relevant role, since we are often interested in minimizing the time for detecting a given threat. This is in contrast to classical detection techniques, where the goal is to maximize the detection probability subject to some probability of false alarm, but where "time" is not explicitly considered. This makes these techniques relevant to applications requiring a time of alert, as generally is the case for safety-of-life users.

One of the most popular techniques of quickest detection is the CUSUM algorithm, which is a sequential method aimed at minimizing the detection delay subject to a false alarm constraint. This method is derived as a solution to "statistical change detection" problems, where the incoming measurements exhibit a sudden change in either their statistical parameters (e.g. mean, variance) or even in the type of its probability density function (e.g. moving from a Gaussian to a uniform distribution). This approach fits very well onto the kind of threats (e.g. interference) that a GNSS receiver may experience in real life, where sudden changes in the properties of the received signal are likely to be experienced.

The quickest detection framework has been extensively studied in the past decades, being applied into a large number of fields [5]. Nevertheless, to the best of the authors' knowledge, quickest detection has not been applied yet to GNSS at signal level. Based on this observation, we already addressed this problem for the case of multi-antenna GNSS receivers (see [6], [7]), and for single-antenna receivers in [8]. Moreover, in [9] we provided a framework to introduce and stimulate the use of quickest detection in GNSS. In this paper, though, we focus only on interference detection for single-antenna GNSS receivers. It is worth noting that none of the above literature presents results with real measurements, which is the main objective of this work. Therefore, our contribution in this work is twofold: (i) to provide a complete set of quickest interference detection techniques able to cope with the wide range of GNSS interference types; (ii) to provide realistic results of the proposed techniques in order to show the capability of our techniques to operate in real working conditions.

Real signals considered in this work were gathered in the framework of the "Integrity Receivers" project (iGNSSrx) funded by the European Commission, being UAB part of the consortium. Thanks to the use of these real data, recommendations are provided herein for setting and tuning the algorithms in practice, when real working conditions need to be faced. The results show that the proposed algorithms can successfully be tuned for different scenarios, and that satisfactory results are obtained, thus paving the way for the implementation of realistic integrity monitoring algorithms.

Next, we introduce the signal model used for developing the detection algorithms. In the following section, we present the quickest interference detectors and their configuration. Finally, we present numerical results obtained with real life signals, showing the capability for detect different kinds of interferences of the proposed approaches.

SIGNAL MODEL

Let us consider a sequence of independent observations $\boldsymbol{x} = [x(0), x(1), \dots, x(v), \dots, x(K-1)]^T$, where v is the time instant at which an integrity threat appears (e.g. interference). Consequently, it is assumed that before v (i.e. at hypothesis $\mathcal{H}_0$) the observation $x(n)$ follows a given statistical distribution, whereas after the change (i.e. at hypothesis $\mathcal{H}_1$) it follows a different one:

$$\begin{aligned} \mathcal{H}_0&: x(n) \sim f_0\big(x(n)\big), \quad n < v \\ \mathcal{H}_1&: x(n) \sim f_1\big(x(n)\big), \quad n \geq v. \end{aligned} \tag{1}$$

Based on these premises, sequential change detection aims at finding the strategy that minimizes the detection delay, while keeping the mean time between false alarms larger than a conveniently set value. For this purpose, the CUSUM algorithm was proposed, which is based on the logarithm of the likelihood ratio, defined by

$$\mathrm{LLR}(n) \doteq \ln \frac{f_1(x)}{f_0(x)} \tag{2}$$

and referred to as the log-likelihood ratio (LLR). For the sake of clarity we have omitted the time index n from the independent random variables x, keeping in mind that each variable correspond to a given time instant (i.e. $x(n)$). For instance, in the case of a Gaussian mean change, where $f_0(x) = \mathcal{N}(\mu_0, \sigma_0^2)$ and $f_1(x) = \mathcal{N}(\mu_1, \sigma_0^2)$, we have the following LLR:

$$\mathrm{LLR}(n) = \frac{\mu_1 - \mu_0}{\sigma_0^2} \cdot \left(x(n) - \frac{\mu_1 + \mu_0}{2} \right). \tag{3}$$

From [9], we know there are two cases:

1) **Completely known LLR**: In this case (i.e. known distributions and parameters), the CUSUM is defined by the next decision rule:

$$g(n) \doteq \big(g(n-1) + \mathrm{LLR}(n)\big)^+ \geq h \tag{4}$$

for some threshold h, where $(x)^+ = \max(0, x)$. By doing so, it is known that the CUSUM algorithm minimizes the detection delay (i.e. $\bar{\tau}$) subject to a constraint in terms of samples between false alarms (i.e. $\overline{T} \geq N_{\mathrm{fa}}$). Actually, the optimality of the CUSUM is achieved with the following results:

$$\begin{aligned} \overline{T} &\geq e^h, \\ \overline{\tau} &\leq \frac{h}{\mathrm{K}[f_1, f_0]}, \end{aligned} \tag{5}$$

with $\mathrm{K}[f_1, f_0] \doteq \mathrm{E}_1[\mathrm{LLR}(n)]$ the Kullback-Leibler divergence, and $\mathrm{E}_1[\cdot]$ the expectation under f_1.

2) **Unknown LLR**: In this case (i.e. when parameters or distribution after change are unknown), we can replace the LLR by any other function of the observations $x(n)$ (i.e. $\rho(n) \doteq q\big(x(n)\big)$), with some negative mean before the change and positive mean after the change (i.e. $\mathrm{E}_0[\rho(n)] < 0$ and $\mathrm{E}_1[\rho(n)] > 0$), as described in [9]. That is,

$$g_{\mathrm{Offset}}(n) \doteq \big(g_{\mathrm{Offset}}(n-1) + \rho(n)\big)^+. \tag{6}$$

In this case, the detection is no longer guaranteed to be optimal, but it is still a very good candidate, provided that an appropriate function is chosen, satisfying:

$$\begin{aligned} \overline{T} &\geq e^{\omega_0 h}, \\ \overline{\tau} &\leq \frac{h}{\mathrm{E}_1[\rho(n)]}, \end{aligned} \tag{7}$$

with $\omega_0 > 0$ the non-zero root of the equation $\mathrm{E}_0\big[e^{\omega \rho(n)}\big] = 1$.

QUICKEST INTERFERENCE DETECTION

Interference detection has been carried out at the output of the GNSS front-end, since it is here where the interference is visible in most cases. In this section we provide different methods for detecting interferences with the aim of detecting a wide range of potential threats. These methods provide different measures (i.e. interference metrics) whose behavior is known when no interference is present and they change when some interference impinges onto the GNSS receiver. The proposed interference metrics can be classified into

- **Statistical metrics**: based on the statistical properties of the samples at the GNSS front-end output.
- **Time-Frequency metrics**: based on the time and frequency characteristics of the received samples.

Variations on the values of these metrics can suggest the presence of an interference threat, thus making these metrics suitable for automatic interference detection. First of all, though, we need to statistically characterize these metrics in order to find the proper CUSUM-type algorithm (i.e. known or unknown LLR) to be used.

To do so, let us define the following signal model. In the absence of interference, the received signal is dominated by noise, since the GNSS signal remains under the noise floor, whereas in the presence of interference, the received signal will be dominated by the interference itself. The detection problem thus becomes:

$$\begin{aligned} \mathcal{H}_0&\colon r(n) = w(n), \\ \mathcal{H}_1&\colon r(n) = i(n) + w(n), \end{aligned} \tag{8}$$

where $r(n)$ is the discrete-time baseband sample at time n, $i(n)$ models the interference, and $w(n)$ is the thermal noise disturbing the received samples, which can be modeled as an independent and identically distributed (i.i.d) zero-mean Gaussian random process with variance σ_w^2.

Statistical Analysis

The statistical analysis is based on the fact that, in absence of interference, the statistical distribution of the samples at the front-end output should resemble a Gaussian distribution. This is so for the case when the automatic gain control (AGC) of the front-end is disabled (i.e. fixed gain) and the dynamic range of the ADC is large enough for resembling the Gaussian distribution. If the AGC is not disabled (i.e. variable gain), we could use the gain indicator evolution instead of the received samples. Henceforth we assume the AGC is disabled and the ADC has enough resolution. Different approaches can be used to measure the degree of Gaussianity, but in this work, we restrict ourselves to three approaches whose combination is able to provide early warnings in case of any kind of potential GNSS interference. These three different approaches are based on the histogram, the kurtosis and the autocorrelation function (ACF) of the front-end output samples, respectively.

Histogram

We know that in the interference free-case, the received signal is dominated by noise, so that the histogram of the received samples should match a Gaussian shape. Meanwhile, when interference is present, the received signal is dominated by the interference, and then the histogram of the received samples should depart from a Gaussian shape. This detection problem is equivalent to a goodness-of-fit test (GoF), in which we are interested on determining whether our received signal follows a Gaussian distribution or not. With this idea in mind, we

propose a method based on a GoF test, which has the advantage of not requiring any a-priori information, and it is applicable to all types of interferences.

This problem was addressed in [9], which uses the following test statistic:

$$x_{hist}(m) = \sum_{i=1}^{N_b} \frac{\left(O_i^{(m)} - E_i\right)^2}{E_i}, \tag{9}$$

with E_i the value of the i-th bin of the reference *theoretical* histogram evaluated under $\mathcal{H}_0$ with N_b bins, and $O_i^{(m)}$ is the value of the i-th bin of the measured histogram with N_b bins at snapshot m, where each snapshot contains N samples of $r(n)$. Moreover, it is shown how the variable $x_{hist}(m)$ under $\mathcal{H}_0$ is approximately chi-squared distributed with $N_b - 1$ degrees of freedom, whereas under $\mathcal{H}_1$ it departs from a central chi-square distribution. That is:

$$\begin{aligned} &\mathcal{H}_0\colon\ x_{hist}(m) \sim \chi^2(N_b - 1), \qquad m < v \\ &\mathcal{H}_1\colon\ x_{hist}(m) \nsim \chi^2(N_b - 1), \qquad m \geq v. \end{aligned} \tag{10}$$

Since the distribution under $\mathcal{H}_1$ is unknown, the LLR cannot be completely defined, and then we must resort to the so-called Offset-CUSUM (see (6)). To do so the function

$$\rho_{hist}(m) \doteq x_{hist}(m) - b \tag{11}$$

is defined, being b a proper offset for which the mean of $\rho_{hist}(m)$ before change (i.e. under $\mathcal{H}_0$) is negative, but it is positive after change (i.e. under $\mathcal{H}_1$) .

Moreover, the choice of the offset b should be large enough to provide a certain false alarm rate through the nonzero root ω_0 with (7), which turns out to be the nonzero root of the next equation:

$$e^{-\omega \cdot b} = (1 - 2\omega)^{\frac{-(N_b-1)}{2}}, \tag{12}$$

which can be solved numerically. Thereby, making use of the decision rule in (6), with $\rho(n)$ defined in (11), we obtain the performance in (7), where ω_0 is the nonzero solution of (12). These bounds, as well as the statistical characterization in (10), were compared in [9] with simulated results, showing a match between the theoretical and simulated results.

Kurtosis

The kurtosis is another metric for measuring the Gaussianity of the data under analysis. It is a statistical value equal to 3 if the data is Gaussian (i.e. under $\mathcal{H}_0$), and otherwise (i.e. under $\mathcal{H}_1$) it departs from 3. Let us define the kurtosis estimate as $\hat{R}(m) \doteq \frac{\hat{\zeta}_4^{(m)}}{\hat{\zeta}_2^{(m)^2}}$, with $\hat{\zeta}_i^{(m)}$ the N-samples estimates of the i-th central moment of the received samples $r(n)$. In turn, m stands for the snapshot index, where each snapshot includes N samples. As for the histogram metric, the kurtosis value was analyzed in [9], which formulates the kurtosis-based detection in a quickest interference detection framework as follows:

$$\begin{aligned} &\mathcal{H}_0\colon\ \hat{R}(m) \sim \mathcal{N}\left(\mu_0^{(\mathrm{k})}, \sigma_0^{2^{(\mathrm{k})}}\right), \qquad m < v \\ &\mathcal{H}_1\colon\ \hat{R}(m) \sim \mathcal{N}\left(\mu_1^{(\mathrm{k})}, \sigma_0^{2^{(\mathrm{k})}}\right), \qquad m \geq v \end{aligned} \tag{13}$$

with mean and variance before change below,

$$\begin{aligned} \mathrm{E}_0\left[\hat{R}(m)\right] &= \mu_0^{(\mathrm{k})} = 3 \cdot \frac{N-1}{N+1}, \\ \mathrm{var}_0\left[\hat{R}(m)\right] &= \sigma_0^{2^{(\mathrm{k})}} = \frac{24}{N}. \end{aligned} \tag{14}$$

Moreover, with the presence of interference , we have the following mean after change:

$$\mu_1^{(\mathrm{k})} = \mu_0^{(\mathrm{k})} \cdot \frac{1 + 2 \cdot \mathrm{INR} + \frac{\mathrm{INR}^2}{2 \cdot dc}}{(1 + \mathrm{INR})^2}, \tag{15}$$

where INR is the interference-to-noise ratio, and dc the duty cycle. This is so for any kind of interference, both pulsed and continuous (i.e. $dc = 1$), except for wide-band ones, which maintain the Gaussianity of the data and then the kurtosis value does not vary.

Hence, from (13) we have characterized the statistical behavior of the kurtosis, with the mean and variance before and after change. Since both moments can be known (i.e. estimated), we are able to fully characterize the LLR as a Gaussian mean change (see (3)), with μ_0, σ_0^2 and μ_1 defined as in (14)-(15), and $x(n) = \hat{R}(m)$ the N-sample kurtosis estimate at snapshot m. Thereby, we can make use of the CUSUM algorithm (see (4)), which leads to the performance in (5), with $\mathrm{K}[f_1, f_0] = \frac{\left(\mu_1^{(\mathrm{k})} - \mu_0^{(\mathrm{k})}\right)^2}{2\sigma_0^{2^{(\mathrm{k})}}}$ the Kullback-Leivler divergence for the kurtosis value. For a detailed analysis of the kurtosis-based detection and the presented results see [9].

ACF

The last statistical analysis considered herein is the one based on the width of the autocorrelation function (ACF). The idea is based on the observation that, in absence of interferences, the samples at the GNSS front-end output are dominated by thermal noise, which exhibits a very narrow ACF. In practice however, the front-end filter will shape the ACF in such a way that a more or less narrow response (depending on the filter bandwidth) will be obtained. On the other hand, the presence of any other signal impinging onto the GNSS receiver will produce additional shapes appearing in the overall ACF of the received samples, which will result in a wider ACF width than that for the interference free case.

Based on the definition of the discrete-time ACF given by $r_r(k) \doteq \mathrm{E}[r(n+k)r^*(n)]$, with $r(n)$ the complex discrete-time samples at the GNSS front-end output, an estimate of the ACF can be obtained as

$$\hat{r}_r^{(m)}(k) = \frac{1}{N} \sum_{n=0}^{N-1} r(n + k + mN) r^*(n + mN), \tag{16}$$

where $m = 0,1,2,\ldots$ stands for the snapshot index, with each snapshot including N samples of $r(n)$, and k is the lag value. With this definition, we can define the ACF width metric as follows:

$$x_{\mathrm{ACF}}(m) \doteq \arg_k \left\{ \frac{\left|\hat{r}_r^{(m)}(k)\right|}{\max_n \left\{\left|\hat{r}_r^{(m)}(n)\right|\right\}} = \frac{1}{e} \right\}. \quad (17)$$

This expression is equivalent to finding the first lag for which the ACF maximum has decreased by a factor e[1]. An important property of this definition is that $x_{\mathrm{ACF}}(m)$ does not depend on the noise power, nor on the number of snapshot samples, but on the bandwidth of the dominant signals. That is to say, when no interference is present, the received samples are dominated by thermal noise and then the width of the ACF depends on the bandwidth of the front-end filter. However, when some interference is present, the ACF width is dominated by the bandwidth of the interference, which is typically smaller than the front-end bandwidth, thus leading to a wider ACF. In general, the ACF width metric will remain constant in both hypothesis $\mathcal{H}_0$ and $\mathcal{H}_1$, but it may slightly vary (one lag up or down) due to possible round-off errors when solving (17). Nevertheless, we can fairly model the ACF width metric as a Gaussian random variable with a small variance to account for the possible round-off errors.

Hence, we can write the following hypotheses, representing the quickest detection framework for the ACF width metric:

$$\begin{aligned} &\mathcal{H}_0\colon x_{\mathrm{ACF}}(m) \sim \mathcal{N}\left(\mu_0^{(\mathrm{A})}, \sigma_0^{2^{(\mathrm{A})}}\right), && m < v \\ &\mathcal{H}_1\colon x_{\mathrm{ACF}}(m) \sim \mathcal{N}\left(\mu_1^{(\mathrm{A})}, \sigma_0^{2^{(\mathrm{A})}}\right), && m \geq v \end{aligned} \quad (18)$$

with $\sigma_0^{2^{(\mathrm{A})}} = 10^{-12}$, $\mu_0^{(\mathrm{A})}$ and $\mu_1^{(\mathrm{A})}$ the value of the ACF width before and after the change, respectively. As we have already said, the ACF width before and after the change is fixed by the front-end and interference bandwidth, respectively. Specifically, the ACF width is the inverse of the front-end bandwidth, and then, since the bandwidth for CW and PW interferences will typically be much smaller, the mean after change (i.e. ACF-width in presence of interference) will be greater than the mean before change.

The previous reasoning relies on the two following considerations:

1) The resolution between lags (i.e. separation between consecutive lags) is lower than the inverse of the front-end filter bandwidth (i.e. $\Delta k < 1/BW$). If this condition is not satisfied, the ACF width in the absence of interference will be fixed by the lag resolution Δk. Thereby, we can write the following condition for the ACF width under $\mathcal{H}_0$:

$$\mu_0^{(\mathrm{A})} = \begin{cases} \dfrac{1}{BW} & \text{if } \Delta k < 1/BW \\ \Delta k & \text{if } \Delta k > 1/BW \end{cases} \quad (19)$$

2) The maximum computed lag (i.e. $k_{\max}$) must be greater than the ACF width under nominal conditions (i.e. in absence of interference) in order to perceive the ACF width change in the presence of interference. Otherwise, the ACF width in presence of interference computed from (17) will be as much equal to $1/BW$, which is the value obtained in the absence of interference.

A common approach in order to calculate the ACF is to calculate (16) for $k = -N, \ldots, 0, \ldots, N$. However, in this way we have to obtain many lags that in general are not providing valuable information (i.e. usually the information is concentrated in the central lags). Therefore, a proper way to proceed is to calculate (16) for a moderate number of lags. To do so, we fix the maximum lag (i.e. $k_{\max}$) and the separation between consecutive lags (i.e. Δk) in order to fix a proper number of lags and a configuration capable of detecting the change on the ACF width in presence of interference (i.e. taking into account the considerations above).

As for the histogram and kurtosis metrics, using (18) we characterize the statistical behavior of the ACF width under the quickest detection framework, with $\mu_0^{(\mathrm{A})}$ known and defined as in (19), $\sigma_0^{2^{(\mathrm{A})}} = 10^{-12}$ and $\mu_1^{(\mathrm{A})}$ dependent on the bandwidth of the interference. Hence, a way to proceed is to fix a certain value for the mean after change according to the minimum change that one expects to detect. In this way, a minimum change detection is set allowing the detection of any larger change caused by different bandwidths. Therefore, we can obtain the exact log-likelihood ratio for a mean Gaussian change as in (3), with means and variance as commented above, and $x(n) = x_{\mathrm{ACF}}(m)$. Thereby, we can use the CUSUM algorithm in (4), leading to the performance in (5). However, in this case, since the variability of the metric is so small, we can fix $h = 1$ and still have a very good performance (i.e. low false alarm rate and detection delay).

Time-Frequency Analysis

Time-frequency analysis (TFA) schemes are based on monitoring the frequency representation of the received signal as a function of time. In the absence of interference, the samples are dominated by noise and thus the frequency representation in the band of interest is usually flat over all frequencies at every time instant. When interference is present, the frequency representation should vary with respect to the flat representation, making possible the interference detection. Different TFA schemes are available in the current literature, but we focus on the spectrogram. The spectrogram is not limited to specific types of interferences, moreover it provides a versatile and affordable approach for interference detection in GNSS. Particularly, when compared to some other much more complex TFA methods such as the Wigner-Ville analysis. It is for this reason that we will use the spectrogram as the de-facto TFA technique herein. In addition, we also include in this section a sequential detection technique based on the estimation of the received power.

Spectrogram

A very simple and widely adopted time-frequency analysis is the short-time Fourier transform (STFT), which leads to the so-called spectrogram, a representation that simultaneously monitors the time- and frequency-domain of the received signal. The spectrogram is obtained through the squared modulus of the Fourier transform of a signal interval. Therefore, at every snapshot, we have an estimate of the power spectral density.

Let us define the discrete spectrogram $S_r(m,f)$ at snapshot m and frequency f of $r(n)$ as follows

$$S_r(m,f) \doteq \frac{1}{N}\left|\sum_{i=1}^{N} r(i+mN-N)e^{-j2\pi\left(\frac{if}{N}\right)}\right|^2, \qquad (20)$$

where $m = 0,1,2,\ldots$ stands for the snapshot index, with each snapshot including N samples of $r(n)$. Therefore, with this expression we have an N-points estimate of the power spectral density every snapshot. We know that in the absence of interference (i.e. under $\mathcal{H}_0$) the spectrogram at snapshot m and frequency f (i.e. $S_r(m,f)$) follows a central χ^2 distribution with two degrees of freedom and proportionality parameter related with the noise power (i.e. σ_w^2). On the other hand, in the presence of interference (i.e. under $\mathcal{H}_1$) it follows a non-central χ^2 with two degrees of freedom, proportionality parameter related to the noise power, and non-central parameter related to the interference power.

This is so because $S_r(m,f) = \frac{1}{N}(\mathbb{R}\mathrm{e}\{y\}^2 + \mathbb{I}\mathrm{m}\{y\}^2)$, with $\mathbb{R}\mathrm{e}\{y\}$ and $\mathbb{I}\mathrm{m}\{y\}$ being Gaussian random variables with variance equal to $N\sigma_w^2$ and mean equal to 0 and $i(n)$, under $\mathcal{H}_0$ and $\mathcal{H}_1$, respectively. These results are obtained taking into account the statistical characterization of $r(n)$ given in (8). Therefore, since both components are quadratically added, the following chi-squared distributions are obtained for $S_r(m,f)$:

$$\begin{aligned} &\mathcal{H}_0\colon\ S_r(m,f) \sim \sigma_w^2 \cdot \chi_2^2, \quad m < v \\ &\mathcal{H}_1\colon\ S_r(m,f) \sim \sigma_w^2 \cdot \chi_2^2(\lambda), \quad m \geq v \end{aligned} \qquad (21)$$

with $\lambda = 2 \cdot \mathrm{INR}$ the non-central parameter of the non-central chi-squared distribution. In order to define a metric to be used in the CUSUM algorithm, we propose the next one:

$$x_{\mathrm{spect}}(m) \doteq \frac{\max_f\left(S_r(m,f)\right)}{\frac{1}{N-1}\cdot\sum_{i=1}^{N-1} S_r(m,f_i)}, \qquad (22)$$

where f_i stands for the i-th frequency bin of the N-points power spectral density defined on (20), excluding the frequency bin of the maximum (i.e. $\max_f(S_r(m,f))$).

The term in the denominator of (22) acts as a normalization factor with respect to the noise power. In this way, we remove the noise dependence of the distribution, and we get a metric that is independent of the noise power. In the absence of interference, the spectrogram is usually flat over all frequencies of interest, and then the maximum value and the mean value will not depart so much one from the other. On the other hand, in the presence of interference, the spectrogram presents peaks in the frequency components of the interference. Hence, the maximum value will now depart considerably with respect to the mean value, and then the spectrogram metric will be much greater than in the absence of interference. Thereby, the spectrogram metric distribution depends on the distribution of the maximum of all frequency bins of the spectrogram (i.e. $\max_f(S_r(m,f))$).

These distributions (i.e. under $\mathcal{H}_0$ and $\mathcal{H}_1$) do not fit the common Gaussian or chi-square distribution, and they have to be analyzed under the framework of extreme value theory. Extreme value theory shows that the cumulative density function (CDF) of the maximum of N independent and identically distributed random variables, with CDF F, has one of three possible functional forms depending on the tail of the parent distribution F. For the chi-square distribution, which is the case of the spectrogram under $\mathcal{H}_0$, the CDF of the normalized maximum in (22) has a double exponential form with the following mean and variance [10]:

$$\begin{aligned} \mu_0^{(s)} &= \ln(N) + \gamma, \\ \sigma_0^{2(s)} &= \frac{\pi^2}{6} = 1.645, \end{aligned} \qquad (23)$$

where γ is the Euler constant with approximate value of 0.5772. Hence, in the absence of interference, the mean value of the spectrogram metric depends on the logarithm of the snapshot samples, whereas the variance is constant.

When the interference is present, the distribution depends on the maximum of a set of non-central chi-square random variables, for which a tractable expression is difficult to find. In that case, the log-likelihood ratio cannot be completely defined, and then we are unable to apply the CUSUM algorithm directly to x_{spect}. An alternative would be to use the Offset-CUSUM variant, because the distribution under $\mathcal{H}_0$ is known (i.e. double exponential with mean and variance as in (23)). However, in order to use the Offset-CUSUM we have to obtain the characteristic function of the distribution under $\mathcal{H}_0$, which is not a straightforward calculation. Hence, in order to avoid this issue, we propose to use a Gaussian mean change CUSUM to detect the change on the mean of the spectrogram metric. In this way, we know that the algorithm may be not optimal (i.e. since the actual distributions are not truly Gaussian), but if the mean change value is properly chosen, the algorithm will perform well using the LLR in (3), with $x(n) = x_{\mathrm{spect}}(m)$, and mean and variance before change defined as in (23) and $\mu_1^{(s)}$ will be experimentally fixed depending on the minimum INR expected to detect.

Thereby, we can make use of the CUSUM decision rule in (4), leading to the following performance:

$$\begin{aligned} \overline{T}_{\mathrm{spect}} &\geq e^{h_{\mathrm{spect}}}, \\ \overline{\tau}_{\mathrm{spect}} &\leq \frac{h_{\mathrm{spect}}}{\mathrm{E}_1\left[x_{\mathrm{spect}}(m)\right]}, \end{aligned} \qquad (24)$$

with $\mathrm{E}_1[x_{\mathrm{spect}}(m)] = \mu_1^{(s)}$ the fixed mean after change. This is so provided that the fixed mean change value is large enough.

Sequential power detection

This section proposes a quickest detection framework for detecting interferences in GNSS, based on the detection of a change in the received power. The detection principle is based on the fact that, in absence of interference, the estimated power should be around the noise power within the corresponding bandwidth. On the other hand, in the presence of some interference the estimated power should significantly deviate from that noise power. This problem was addressed in [8], which defined the following detection metric:

$$x_{RX}(m) \doteq \frac{\hat{P}_{\mathrm{RX}}(m)}{2\sigma_w^2}, \tag{25}$$

with $\hat{P}_{\mathrm{RX}}(m)$ the estimated receiver power at snapshot m.

This metric can be statistically characterized as [8]:

$$\begin{aligned} &\mathcal{H}_0\colon\ x_{\mathrm{RX}}(m) \sim \mathcal{N}\left(\mu_0^{(r)}, \sigma_0^{2^{(r)}}\right), \quad m < v \\ &\mathcal{H}_1\colon\ x_{\mathrm{RX}}(m) \sim \mathcal{N}\left(\mu_1^{(r)}, \sigma_1^{2^{(r)}}\right), \quad m \geq v \end{aligned} \tag{26}$$

with expressions for the mean and variance as follows:

$$\begin{aligned} &\mu_0^{(r)} = 1 \qquad && \sigma_0^{2^{(r)}} = \frac{1}{N} \\ &\mu_1^{(r)} = (1 + \mathrm{INR}) \qquad && \sigma_1^{2^{(r)}} = \frac{1}{N} \cdot (1 + 2 \cdot \mathrm{INR}). \end{aligned} \tag{27}$$

From (26) we have statistically characterized the power estimate metric, including the mean and variance before and after change defined in (27). Therefore, we can fully characterize the log-likelihood ratio, and then use the CUSUM algorithm for detecting both changes in the mean and variance. This gives rise to the following LLR:

$$\begin{aligned} \mathrm{LLR}_{\mathrm{r}}(m) = \ln\left(\frac{\sigma_0^{2^{(r)}}}{\sigma_1^{2^{(r)}}}\right) + \frac{\left(x_{\mathrm{RX}}(m) - \mu_0^{(r)}\right)^2}{2\sigma_0^{2^{(r)}}} \\ - \frac{\left(x_{\mathrm{RX}}(m) - \mu_1^{(r)}\right)^2}{2\sigma_1^{2^{(r)}}} \end{aligned} \tag{28}$$

with the means and variances defined above. Hence, we can make use of the CUSUM algorithm as in (4), using the above LLR, and then leading to the performance in (5), with $\mathrm{K}[f_1, f_0] = \ln\left(\frac{\sigma_0^{(r)}}{\sigma_1^{(r)}}\right) + \frac{\left(\mu_1^{(r)} - \mu_0^{(r)}\right)^2}{2\sigma_0^{2^{(r)}}}$. For further analysis on the received power metric and the presented results see [8].

REAL DATA ANALYSIS

This section shows the results of the detection algorithms previously proposed, using real (i.e. live) signals captured in the framework of the EC funded Integrity GNSS Receiver (iGNSSrx) project. Specifically, a measurement campaign was done, comprising real signals captured with a GNSS receiver at the Joint Research Center (JRC) in order to analyze the interference detection algorithms in practice. The used receiver captured GPS L1 signals with the following features: bandwidth of 4MHz, sampling rate of 10MHz, intermediate frequency of 2.57MHz and 8 quantification bits. We divide the results according to the different interference signals, which include the most prevalent and dangerous types of interferences that we can find in GNSS (i.e. continuous wave, pulsed wave and Gaussian wide band interferences). Actually, chirp interferences are also common and were also captured at the JRC. However, we do not present here the results because they can be inferred from that obtained with continuous and pulsed wave interferences. Then, for each one we show the results of the quickest detection algorithms. In fact, we show the more relevant metrics for each type of interference.

The presented results include the statistical characterization (i.e. histogram) of the methods for both presence and absence of interference. Moreover, they include the evolution of the sequential metric. This is obtained by processing 2 minutes of the real signals data, whose first minute includes the absence of interference case, and the last minute includes the presence of interference case. The snapshot time is fixed to 20ms, which is a common used value in practice by receivers and it is a convenient snapshot in order to get a sufficient large value for the snapshot samples assuring the results previously presented.

Continuous Wave Interference (CW)

Next, we show the results after processing an in-band CW. This interference can be detected by any of the proposed methods, but we only show the histogram and ACF metrics. Specifically, the interference starts being detected when it takes an INR = 4dB. However, here, we show the results for the case of INR = 24dB. This is so because in this way we can clearly see the change in the metrics when the interference appears. Moreover, this value fits well with the range of values we can encounter in practice, since the interference power is much greater than the noise level.

Basically, we will see next that the statistical characterization of the histogram-based detection metric does not fit at all with the one theoretically stated (i.e. chi-square). Nevertheless, the detection algorithm still works pretty well by properly setting the offset b (see (11)). As for the ACF width, we will see that behaves as expected.

Histogram-based detection

Here, we present the results for the histogram-based detection metric and show the detection process by using this metric. Figure 1 shows the statistical characterization of the histogram metric for both absence (left) and presence of the CW interference with INR = 24dB (right). We can see how the histogram in both cases is quite different. Thus, the histogram metric exhibits a large change that allows the detection of the interference. The results are obtained by using 100 bins for computing the

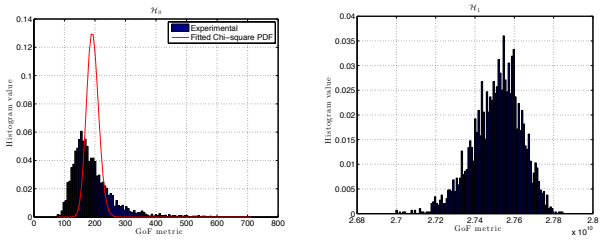

Figure 1 Statistical characterization of the Histogram-based detection metric for the CW.

histogram (i.e. $N_b = 100$). In the left plot we can see how the experimental distribution of the histogram metric does not fit the theoretical chi-square distribution. The fitted chi-square distribution is a chi-square distribution with degrees of freedom equal to the mean of the metric. This fitted PDF corresponds to the theoretical one since the mean of a chi-square distribution is equal to the degrees of freedom. The fact that the experimental and theoretical characterizations do not fit may be due to the fact that the distribution of the received signal in absence of interference is not actually a zero-mean Gaussian distribution.

We analyzed different sets of data and we realized that the mean of the metric for different snapshot times is around $2 \cdot N_b$. Then, as the CUSUM algorithm for the histogram is based on the Offset-CUSUM, we can still use the proposed method but taking into account that the mean before the change is equal to $\mu_0 = 2 \cdot N_b$ instead of being equal to $N_b - 1$, and using an offset $b = 5 \cdot \mu_0$ in order to make sure that the metric is negative in the absence of interference.

Figure 2 shows the histogram-based detection metric and the CUSUM time-evolution. In the left plot we see how the histogram metric changes just when the interference appears (i.e. second 60). The value after change will depend on the INR since the increment of the INR leads to an increment on the effects of the interference, and subsequently, an increment of the detection metric. Finally, in the right plot, we can see the CUSUM time-evolution. In the absence of interference, it is close to 0, whereas just at the change time, it increases and crosses the threshold, clearly indicating the presence of interference.

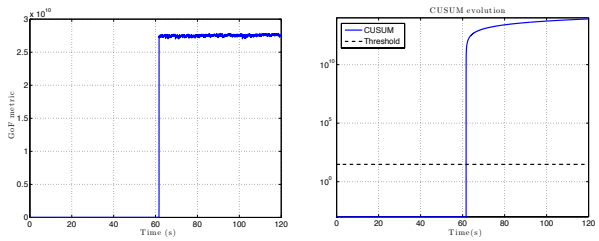

Figure 2 Interference detection for the CW. Metric (left) and CUSUM time-evolution (right).

These results are obtained tuning the algorithm as follows:

- We set the degrees of freedom to $2N_b$, with $N_b = 100$ bins. Then, we have a mean before the change equal to $\mu_0 = 2N_b$.
- We use an offset $b = 5\mu_0$, which is large enough to maintain a negative mean before change and it is short enough to maintain a positive mean after change (see Figure 1).
- We fix the threshold $h_{\text{hist}} = \ln\left(\frac{N_{fa}}{\omega_0}\right)$, with N_{fa} the number of desired metric samples between false alarms and ω_0 the non-zero root of (12).
- Finally, we use the decision rule in (6).

ACF-width-based detection

Here, we present the results for the ACF width detection metric. Figure 3 shows the ACF behavior under $\mathcal{H}_0$ and $\mathcal{H}_1$ in the left plot, whereas in the right plot is shown the ACF width evolution in time. For the ACF calculation we use $k_{\max}$ =1ms and $\Delta k = 20\mu$s. In the left plot, we see how the ACF under $\mathcal{H}_0$ (red curve) decays abruptly when the time delay departs from 0. Indeed, the ACF falls below the 1/e factor just for the first computed lag. On the other hand, for $\mathcal{H}_1$ we see that the ACF remains above the factor 1/e for all the computed range (i.e. $\pm k_{\max}$).

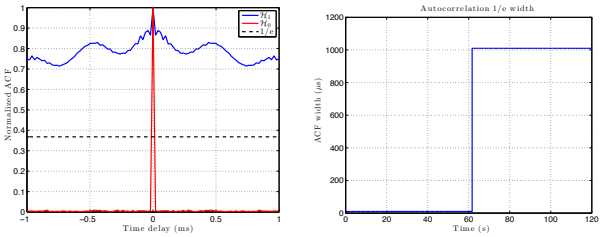

Figure 3 ACF for the CW1 (left) and ACF width time-evolution (right).

Hence, the ACF width exhibits a change in the presence of interference that allows us to detect it, as can be seen in the right plot of Figure 3. We see how the ACF width takes an abrupt change just when the interference appears (i.e. 60-th second). The value obtained under $\mathcal{H}_0$ is equal to the lag resolution (i.e. 20μs), whereas when the interference appears it takes a value of 1ms. This is so because, as shown in the left plot, the ACF does not decay by a factor 1/e anywhere within the computed range. Therefore, as the computed range extends from $-k_{\max}$ to $k_{\max}$, the obtained ACF width is equal to $k_{\max}$. In this case, the value under $\mathcal{H}_1$ does not vary with the INR. This is so because the ACF width basically depends on the interference shape, which is independent of the interference power, and then the shape and the ACF width remains constant with the variation of the INR.

Here we do not show the CUSUM behavior because it is similar to that obtained for the histogram case (see Figure 2). The tuning of the CUSUM algorithm becomes the following:

- We set the mean and variance before change to $\mu_0^{(A)} = \Delta k$ and $\sigma_0^{2(A)} = 10^{-12}$, respectively, with Δk the separation between obtained lags in the ACF calculation from (16).
- We set the mean after change to $\mu_1^{(A)} = 5 \cdot \mu_0^{(A)}$ and fix the threshold to $h_{\text{ACF}} = 1$.
- Finally, we use the LLR for the Gaussian mean change in (3), with $x(n) = x_{\text{ACF}}(m)$ in (17), and then we use the decision rule in (4).

Pulsed Sinusoidal Interference (PW)

Next, we show the results of the pulsed sinusoidal interferences. We present two different interferences each one with a different duty cycle, in order to see the corresponding effects of onto the detection metrics. In fact, we have chosen, among the generated interferences, the lowest (i.e. 0.98%) and greatest (i.e. 30%) duty cycle, which correspond to a small and large pulse width, respectively. We will denote the two interferences as PW1 and PW2, respectively. Moreover, we show the results for INR = 14dB. We present the results for the kurtosis- and spectrogram-based detection, which are the most relevant metrics for detecting PW interferences.

Kurtosis-based detection

Figure 4 shows the statistical characterization of the kurtosis metric for PW1. In the left plot we observe how the histogram under $\mathcal{H}_0$ takes a Gaussian shape, with mean 3 and variance approximately equal to 5e-4, whereas using the theoretical expression in (14), with a snapshot of 20ms and sampling rate of 10MHz, we obtain a value of 1.2e-4. This is so because, in fact, the value of N in the expression of the variances refers to the number of independent samples that were used to calculate the kurtosis estimate. Then, as in our case the signal samples are filtered by a baseband bandwidth of $B = 2$MHz, not all the samples in a snapshot period are independent, since they will be correlated by the filter shape.

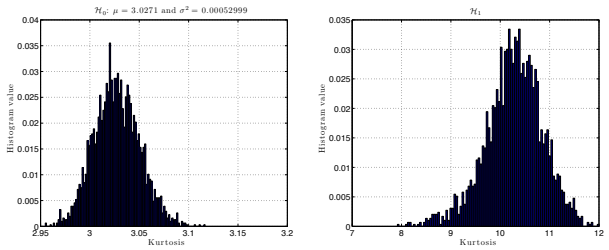

Figure 4 Statistical characterization of the Kurtosis estimation for the PW1.

In order to obtain the proper variance value we would have to define the number of independent samples as $N = N_{sp} \cdot \left(\frac{B}{F_s}\right)$, with $N_{sp} = F_s \cdot T_{sp}$, where F_s and T_{sp} are the sampling rate and snapshot time, respectively. In our case, we obtain a factor 0.2 multiplying the snapshot samples. Substituting this effective number of samples into the variance expression we obtain the factor 5 that makes fit both experimental and theoretical results (i.e. $\sigma_0^{2(k)} = 5 \cdot \frac{24}{N_{sp}}$). On the other hand, in the right plot of Figure 4 we see how the histogram presents a change in the mean under $\mathcal{H}_1$. Moreover, we see how the histogram seems to be Gaussian, but presenting a large left tail. This is so because the kurtosis varies between two values due to the variation of the effective duty cycle from different snapshots.

Figure 5 shows the time-evolution of the kurtosis metrics for PW1 and PW2. We see how in both cases the metric varies between two different values after the change. This is due to the effect mentioned before on the duty cycle variation. Moreover, these values are around 10 and 5, which are close to the value obtained using the theoretical expression in (15) taking into account the effective INR (i.e. multiplied by the duty cycle). With these values we see that the lower the duty cycle, the larger the kurtosis value. Therefore, in order to fix the minimum change level for the CUSUM configuration, we should take into account the kurtosis value for the case of large duty cycle. Doing so, we will be able to detect any PW interference with any smaller duty cycle, since they will produce a larger change, thus becoming detectable.

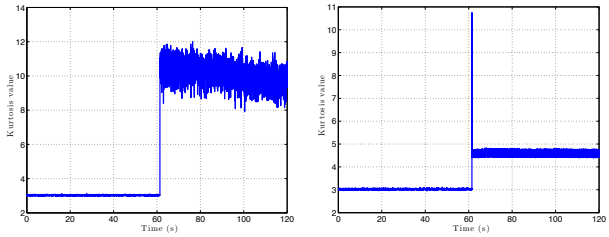

Figure 5 Kurtosis time-evolution for the PW1 (left) and PW2 (right).

In view of the discussion above, we can configure the kurtosis-based CUSUM as follows:

- We set the mean and variance before change to $\mu_0^{(k)} = 3$ and $\sigma_0^{2(k)} = 5 \cdot \frac{24}{N_{sp}}$, respectively, with N_{sp} the number of samples in a snapshot.
- We set the mean after change to $\mu_1^{(k)} = 4$, which is the theoretical value for a PW with INR = 14dB and duty cycle of 30%, and fix the threshold $h_{\text{kurt}} = \ln(N_{fa})$, with N_{fa} the number of desired **metric** samples between false alarms.
    - This value for the mean after change is for the case of a PW. If the interference is a CW, the mean change is negative (i.e. the mean after change is lower than before change), and then we have to use another CUSUM tuned with the proper mean after change (e.g. $\mu_{1_{CW}}^{(k)} = 2.6$).
- Finally, we use the LLR for the Gaussian mean change in (3), with $x(m) = \hat{R}(m)$, and then we use (4).

Spectrogram-based detection

Here, we show the results of the spectrogram metric for the PW interference. Figure 6 shows the statistical characterization of the spectrogram metric. In the left plot we present the histogram in the absence of interference, and the value for the mean and variance before the change. Among the analyzed data, we see that the mean of the spectrogram metric in the absence of interference is around 9, whereas the variance value is about 0.2. On the other hand, in the right plot, we see how the histogram of the spectrogram metric under $\mathcal{H}_1$ departs from that under $\mathcal{H}_0$. Since the distributions in both hypotheses are unknown, the most important thing here is to see the large change in the mean of the metric, and then the use of mean change CUSUM is coherent.

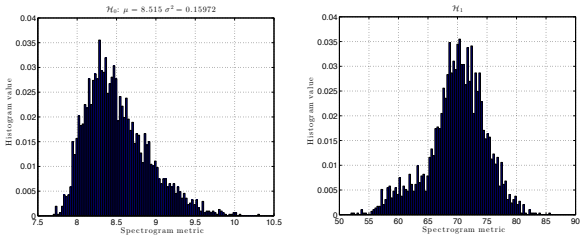

Figure 6 Statistical characterization of the spectrogram metric for the PW1.

In this case, the change value depends on the INR as well as the duty cycle, since depending on the ON state time of the pulsed interference the peak appearing in the spectrogram will be more or less large, therefore producing a greater or smaller value after change. This is shown in Figure 7, which presents the evolution in time of the spectrogram metric for the PW1 and PW2 (i.e. short and large duty cycle). We see how the metric varies between two different values after the change, as for the kurtosis case. Therefore, in order to fix the minimum change level we should use the one obtained with the lower duty cycle (i.e. lower change). Thereby, we may use a minimum change level of 50 in order to allow the detection of the PW1. This minimum change level is good since it fulfills the condition $\mu_1^{(s)} > 5 \cdot \mu_0^{(s)} = 45$ needed to obtain a good performance of the mean change CUSUM algorithm (see Spectrogram section).

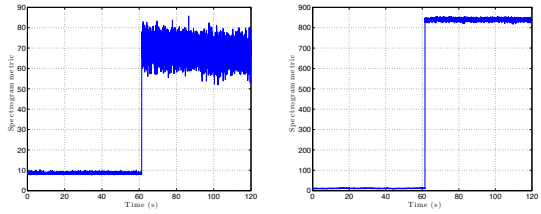

Figure 7 Spectrogram-based metric time-evolution for the PW1 (left) and PW2 (right).

Hence, we can configure the spectrogram-based CUSUM as follows:

- We set the mean and variance before change to $\mu_0^{(s)} = 9$ and $\sigma_0^{2(s)} = 0.2$, respectively.
- We set the mean after change to $\mu_1^{(s)} = 50$ and fix the threshold $h_{\text{spect}} = \ln(N_{fa})$.
- Finally, we use the LLR for the Gaussian mean change in (3), with $x(n) = x_{\text{spect}}(m)$ defined in (22), and then we use the decision rule in (4).

Wide Band Interference (WB)

This section is dedicated to present the results of a wide band interference corresponding to a Gaussian signal of 50MHz centered in-band (i.e. at 1.575420 GHz). We process all the INR available in the captured data, which starts with the absence of interference and then gradually increases in steps of 5dB (-71, -16, -11, -6, -1, 4, 9, 14, 19, 24dB). The interference introduces slight variations into all the metrics, except for the ACF width and spectrogram metrics. However these variations are clearly detectable by the histogram- and received power-based detection, which are shown in this section.

Since the interference is Gaussian, it is striking that it is detectable by the histogram-based metric, as the Gaussianity of the received signal samples is maintained even with interference, and then the statistical analysis metrics should not vary. However, for the histogram metric, the presence of interference is translated into an increase of the variance of the received signal samples (i.e. increase of the noise power). Therefore, if we know the noise power under ideal conditions (e.g. we estimate it), the presence of the wide band interference spreads the histogram of the received samples, and then the histogram-based metric will depart from the ideal conditions value. The same happens with the received power metric, if we know the noise power under ideal conditions, we are able to discriminate an increase of this power due to the presence of interference.

Histogram-based detection

Here, we present the results for the histogram metric. Figure 8 shows the detection metric and the CUSUM time evolution. In the left plot we see how as the INR increases (5dB every minute) the histogram metric does so. In fact, due to the huge change in the metric we do not see when actually the metric starts to change. Specifically, the metric takes a slight variation around 120 seconds, which is due to the interference with INR = -11dB. However, the change is not substantial until about 180 seconds (i.e. INR =-6dB). It is for this reason that the CUSUM algorithm starts detecting the interference around 180s (see right

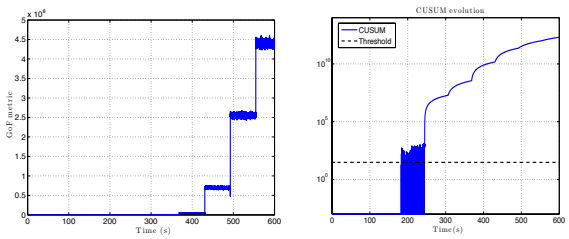

Figure 8 Metric time-evolution (left) and CUSUM decisions (right) for the WB interferences.

Table 1 Properties of the suggested interference detection algorithms

Metric	HISTOGRAM	KURTOSIS	POWER
CUSUM type	Bias-CUSUM	Mean-change	Mean&variance-change
Detection delay	Large	Medium	Small
Target interferences	All	All except wideband	CW, wideband.
Fixed parameters	None	$\mu_{CW/PW}^{(kurt)} = 2.2/4$	$\mu_1^{(RX)} = 3,\ \sigma_1^{(RX)} = 2e-4$
Noise dependence	Yes	No	Yes
Threshold	$h = \ln\left(\frac{\bar{T}}{\omega_0}\right),$ $\bar{\tau} \leq \frac{\ln\left(\frac{\bar{T}}{\omega_0}\right)}{\mu_1}$	$h = \ln(\bar{T}),$ $\bar{\tau} \leq \frac{\ln(\bar{T})\cdot 2\sigma_0^2}{(\mu_1-\mu_0)^2}$	$h = \ln(\bar{T}),$ $\bar{\tau} \leq \frac{\ln(\bar{T})}{\ln\left(\left\|\left(\frac{\sigma_0}{\sigma_1}\right)\right\|\right)+\frac{(\mu_1-\mu_0)^2}{2\sigma_0^2}}$

plot of Figure 8). Nevertheless, the CUSUM is changing of decision among the time the interference with INR = -6dB is present. This is so because the change is not large enough to maintain a mean after change positive, and then there are some snapshots where the metric is small enough to make the CUSUM decides to absence of interference. Hence, is not until about 240 seconds (i.e. INR = -1dB) when the CUSUM detects the interference among the entire interval.

Power-based detection

Here, we present the results for the power-based detection. Figure 9 shows the statistical characterization of the power metric. As for the other methods, we present in the left plot the histogram under $\mathcal{H}_0$, and in the right plot the one when the WB is present with INR = 24dB. We see how for the ideal conditions, the expressions for the mean and variance before the change in (27) are approximately equal to the experimental results (i.e. $\mu_0^{(r)} \approx 1$, $\sigma_0^{2^{(r)}} = 4.4e-5$). On the other hand, we see in the right plot how the histogram significantly changes in the presence of interference, and then it becomes detectable, as we expected. In this case, though, the relationship between the theoretical and experimental results does not match exactly. This is so because the wide band interference is filtered with a lower bandwidth, and then the power is reduced.

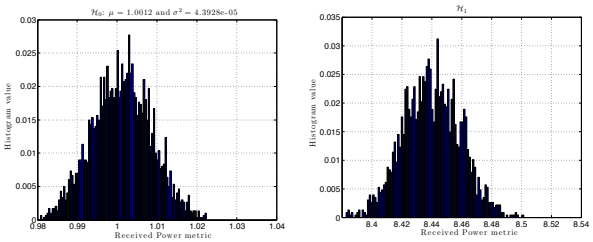

Figure 9 Statistical characterization of the Power metric for the WB interference.

Figure 10 shows the evolution in time of the power metric and the CUSUM. In the left plot, we see how the change on the metric increases as the INR of the interference does so, but as we said, the change is not as big as the expected one with the given INR. Nevertheless, with a minimum change fixed to 3 (i.e. 3dB) the interference is detected around second 360 (i.e. INR = 4dB). As for the histogram

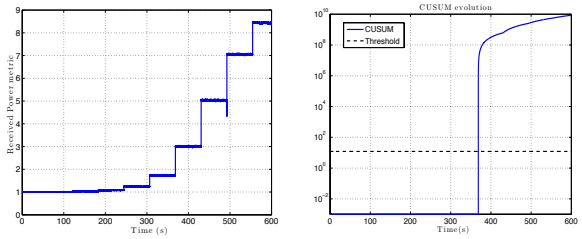

Figure 10 Power metric time-evolution (left) and CUSUM decisions (right) for the WB interference.

case, the power metric starts changing before second 360, and this can be detected by decreasing the minimum change fixed. However, detecting an interference with INR=4dB is enough for practical situations, since interferences will often appear with powers much greater than just 4 dB above the GNSS received power levels.

Therefore the minimum change fixed to 3 is a proper value for detecting interferences with low INR and provides a good level of false alarms rate. This is because decreasing the minimum change level would detect lower INR, but at the expense of increasing the number of false alarms. Hence, we can configure the power-based CUSUM as:

- We set the mean and variance before change to $\mu_0^{(r)} = 1$ and $\sigma_0^{2^{(r)}} = 5 \cdot \frac{1}{N_{sp}}$, respectively.
- We set the mean and variance after change to $\mu_1^{(r)} = 3$ and $\sigma_1^{2^{(r)}} = 5 \cdot \frac{5}{N_{sp}}$ and fix the threshold to $h_{\mathrm{RX}} = \ln(N_{fa})$.
- Finally, we use the LLR for the Gaussian mean and variance change in (28), with $x_{\mathrm{RX}}(m)$ in (25), and then we use the decision rule in (4).

CONCLUSIONS

Based on the results presented so far, we can summarize the main features of the proposed techniques in terms of their suitability to certain scenarios, the type of sequential algorithm they implement, and their main configuration parameters. A summary of the proposed interference detection techniques is provided in Table 1 for the case of the histogram, kurtosis and power tests, which are the selected signal processing techniques for providing a complete set in order to be able to detect all types of interferences. The ACF-width and TFA metrics are

discarded due to their higher computational load, and the fact that they do not provide additional information that may relevant for detection purposes. Regarding the histogram, it is based on the Bias-CUSUM, for which we only need to know the statistical characterization of the interference-free scenario (i.e. $\mathcal{H}_0$ hypothesis). This has the advantage of reducing the number of parameters to be tuned, but at the same time, it departs from the conventional CUSUM approach and thus incurs in a larger detection delay.

Instead, the mean-change (MC) and mean&variance-change (MVC) CUSUM implemented for the kurtosis and power tests, respectively, do provide the quickest detection by minimizing the detection delay. For the power test, this is particularly true for CW and wideband interference, since these are the interferences for which the test has been specifically designed (i.e. using the mean and variance values in Table 1). For the kurtosis test, wideband interferences (particularly those occupying the whole front-end bandwidth) are the ones that cannot be detected because they are often perceived just as an increased noise level. Regarding the noise, it should be mentioned that all the proposed techniques except for the kurtosis, do depend on the noise power, but this has already been taken into account when processing the data measurements. The CUSUM parameters are also indicated in Table 1. As we already said, for the histogram we do not need to fix a minimum change magnitude. For the kurtosis, after analyzing all the results, a proper mean after change is 2.2 and 4 for the CW and PW-CUSUM, respectively. Those values belong to a minimum INR detectable of 4dB for the CW case and of 10dB and duty cycle equal to 0.25 for the PW case. On the other hand, for the power metric, we suggest a mean and variance after change of 3 and 2e-3, respectively, which correspond to a minimum detectable INR of 3dB.

Finally, the last row of Table 1 shows the selected threshold as a function of the metric samples between false alarms (i.e. $\bar{T} = t_{fa}/T_{sp}$, with t_{fa} the time between false alarms in seconds). Moreover, we also provide the corresponding bound for the detection delay, which depends on the false alarm rate and the CUSUM parameters. For the histogram case, the threshold depends on both the false alarm rate and the non-zero root ω_0, which is calculated from (12). On the other hand, the threshold for both the kurtosis and power metric depends on the false alarm rate, only. Since the non-zero root ω_0 is smaller than one, for the same false alarm rate, the threshold of the histogram metric algorithm will be larger than that obtained for the kurtosis and power metrics. For the same reason we can say that the CUSUM algorithm for the kurtosis and power metric will be quicker than the histogram metric algorithm. In addition, if we analyze the detection delay for the kurtosis and the power metric, we see that the denominator of the power metric delay is greater than the one for the kurtosis metric algorithm. Therefore, the detection delay for the power metric is shorter than the kurtosis metric one.

ACKNOWLEDGEMENTS

This work was partly supported by the Spanish Government under grant TEC2014-53656-R and by the European Commission under the iGNSSrx project (ENTR/129/PP/ENT/SP2/11/6602). Also we would like to thank all the reviewers of this work for the valuable comments. In particular, we would like to thank Elisa Guzman Alonso for her valuable review.

REFERENCES

[1] B. W. Parkinson and J. J. Spilker, *Global Positioning System: Theory and Applications vol.2*. Aiaa, 1996.

[2] G. Seco-Granados, *et al.*, "Challenges in Indoor Global Navigation Satellite Systems," *IEEE Sig. Proc. Mag.*, vol 29, no. 2, pp. 108–131, 2012.

[3] M. Thomas, *Global Navigation Space Systems: reliance and vulnerabilities*, vol. 24, no. 9. The Royal Academy of Engineering, 2011.

[4] A. T. Balaei and A. G. Dempster, "A statistical inference technique for GPS interference detection," *IEEE Trans. Aerosp. Electron. Syst.*, vol. 45, no. 4, p. 1499, 2009.

[5] M. Basseville and I. V Nikiforov, *Detection of Abrupt Changes: Theory and Application*. 1993.

[6] D. Egea, *et al.*, "Single- and Multi-Correlator Sequential Testsfor Signal Integrity in Multi-Antenna GNSS Receivers," in *ICL-GNSS*, 2014.

[7] D. Egea, *et al.*, "Interference and multipath sequential tests for signal integrity in multi-antenna GNSS receivers," in *IEEE SAM,* 2014.

[8] D. Egea-Roca, *et al.*, "Quickest Detection Framework for Signal Integrity Monitoring in Low-Cost GNSS Receivers," in *IEEE VTC (accepted)*, 2015.

[9] D. Egea-Roca, *et al.*, "On the Use of Quickest Detection Theory for Signal Integrity Monitoring in Single-Antenna GNSS Receivers," in *ICL-GNSS (accepted)*, 2015.

[10] S. Turunen, "Network Assistance What Will New GNSS," *Insid. GNSS*, vol. 2, no. 3, pp. 35–41, 2007.